Coordinative Reduction of Metal Nodes Enhances the Hydrolytic Stability of a Paddlewheel Metal–Organic Framework

Dahae Song,[†] Jinhee Bae,[†] Hoon Ji,[†] Min-Bum Kim,[‡] Youn-Sang Bae,[‡] Kyo Sung Park,[§] Dohyun Moon,*[,||] and Nak Cheon Jeong*[,†]

[†]Department of Emerging Materials Science, DGIST, Daegu 42988, Korea
[‡] Department of Chemical and Biomolecular Engineering, Yonsei University, Seoul 03722, Korea
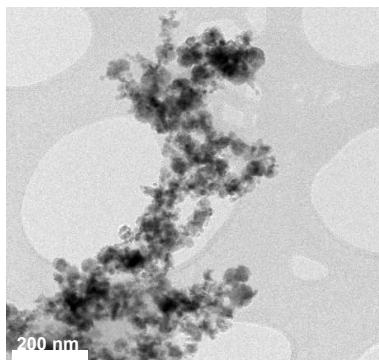[§]Research Park, LG Chem, Seoul 07796, Korea
[||]Beamline Department, Pohang Accelerator Laboratory, Pohang 37673, Korea

*To whom correspondence should be addressed.   E-mail: nc@dgist.ac.kr; dmoon@postech.ac.kr

Table of Contents

Section S1. TEM Analysis of HKUST-1 After LiBH$_4$ Treatment

Figure S1. A TEM image of LiBH$_4$-treated HKUST-1.   HKUST-1 are decomposed, forming Cu^0 nanoparticles.

Section S2. Topological View of HKUST-1

HKUST-1 has two types of large cages with the shape of a truncated cube (type 1 and type 2 cages) and a type of corner-sharing small cage with the shape of a truncated octahedron (a type 3 cage) (see Figure S2 below). Three-dimensional type 1 and type 2 large cages are alternately interconnected and share large windows.   The small cages (type 3) formed at the edges of large cages share small windows with type 2 large cages.
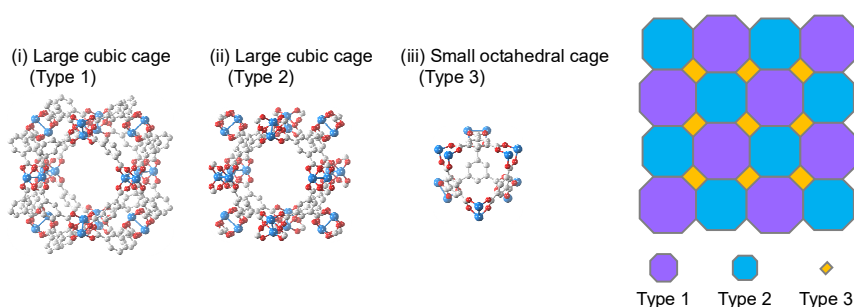
Figure S2. Illustrations of three types of cages in HKUST-1 and a 2-dimensional representation of the topological arrangement of the cages.
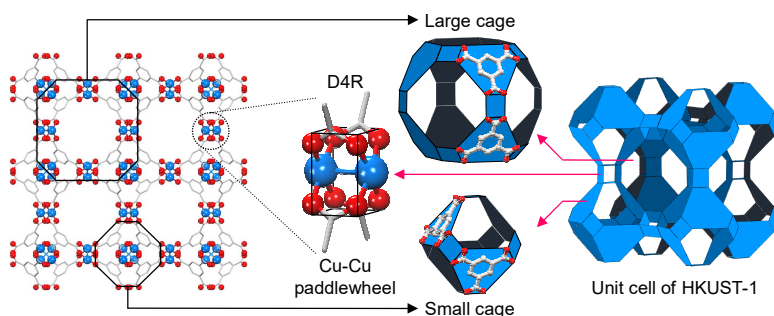
Figure S3. Crystal structure of HKUST-1 framework and 3-dimensional illustration of the unit cell and building units of HKUST-1.   Cu−Cu paddlewheel node in a D4R secondary building unit constitutes the wall of a large cubic cage as well as a small octahedral cage in HKUST-1.   Hydrogen atoms bound to carbon atoms in the benzene moieties are omitted for the sake of clarity.

Section S3. Materials and Methods

Materials.   All reagents were obtained from commercial sources (Sigma Aldrich, Alfa Aesar, or Daejung). Copper (II) nitrate hemipentahydrate [$Cu(NO_3)_2 \cdot 2.5H_2O$, 98.0-102%, Aldrich], trimesic acid (1,3,5-bezenetricarboxylic acid, BTC, 95%, Aldrich), ethanol (EtOH, 94.5%, Daejung), N,N-dimethylformamide (DMF, 99.5%, Daejung), and distilled deionized water (DDW) were used for the synthesis of HKUST-1 powder.   Copper(II) Chloride dihydrate [$CuCl_2 \cdot 2H_2O$, 99%, Aldrich] and hydrochloric acid (HCl, 37%, Sigma Aldrich) were additionally employed for the synthesis of large single crystals of HKUST-1. Hydroquinone (H_2Q, 99.5%, Aldrich) and anhydrous acetonitrile (MeCN, 99.8%, Aldrich) were used for the H_2Q treatment of HKUST-1.   The MeCN was distilled and purified with activated zeolite 4A in a moisture-free argon-filled glove box prior to use.   Deuterated sulfuric acid (D_2SO_4, 96-98 wt% in D_2O, 99.5 atomic % in deuterium, Aldrich) and deuterated acetonitrile (MeCN-d_3, 99%, Aldrich) were, respectively, used for dissolving HKUST-1 and H_2Q before performing the ^{1}H-nuclear magnetic resonance (^{1}H NMR) spectroscopic analysis.   All synthesized MOFs were stored in a moisture-free argon-filled glove box before use.

Synthesis of HKUST-1 powder.   We synthesized HKUST-1 following the procedure described in our previous reports.[S1]   Briefly, $Cu(NO_3)_2 \cdot 2.5H_2O$ (0.87 g, 3.6 mmol) was dissolved in 10 mL of DDW in a vial. In a separate vial, BTC (0.22 g, 1.0 mmol) was dissolved in 10 mL of EtOH.   The $Cu(NO_3)_2$ solution was quickly added into the vial containing the BTC solution.   After the mixed solution was continuously stirred for 10 min at room temperature, 1 mL of DMF was added into the mixed solution.   Then, the vial was sealed with polytetrafluoroethylene (PTFE) tape.   The vial was placed in an oven at 80 °C for 20 h to allow the mixture to react.   After the product cooled to room temperature, we collected and washed the crystalline solid (pristine HKUST-1) with a mixed solvent of H_2O and EtOH.

Synthesis of HKUST-1 large single crystal.   HKUST-1 large single crystals were synthesized with a similar procedure described above except using $CuCl_2$ instead of $Cu(NO_3)_2$ and adding HCl. $CuCl_2 \cdot 2H_2O$ (1.47 g, 8.6 mmol) was dissolved in 200 mL of DDW in a glass bottle.   Then, 2.20 g of DMF was added into the $CuCl_2$ solution.   After BTC (2.10 g, 10 mmol) was dissolved in 200 mL of EtOH in a separate glass bottle, 0.25 g of HCl was added into the BTC solution.   Then, the $CuCl_2$ solution was quickly added into the bottle containing the BTC solution.   After the bottle was sealed with polypropylene cap and PTFE tape, the bottle was placed in an oven at 80 °C for 5 d to allow the mixture to react.   After the product cooled to room temperature, we collected and washed the pristine HKUST-1 large crystals with a mixed solvent of H_2O and EtOH.

Thermal activation (TA) of HKUST-1.   Coordinated H_2O and EtOH solvents in pristine HKUST-1 were removed by TA before the H_2Q-treatment of HKUST-1 (hereafter we call H_2Q-treated HKUST-1 as H_2Q-HK). For the TA of pristine HKUST-1, a pristine HKUST-1 sample was placed in a glass vacuum tube.   Then, the tube was heated at 150 °C for 24 h under vacuum (~10^{-3} Torr).   After cooling down to room temperature, the tubes were transferred into a moisture-free argon-charged glove box.

H_2Q-treatment of HKUST-1.   0.50 g of the thermally activated HKUST-1 was placed in a 20 mL vial.   In a separate vial, we prepared H_2Q solution by dissolving 0.137 g of H_2Q in 20 mL of purified MeCN.   After the H_2Q solution was added into the vial containing activated HKUST-1, the vial was placed on a hotplate at 80 °C for 12 h to allow the H_2Q to react with HKUST-1.   After the vial cooled to room temperature, we collected and washed the H_2Q-HK crystals with the purified MeCN.   We repeated this process four more times only by replacing fresh H_2Q/MeCN solution to investigate whether all Cu^{2+} ions can be reduced to Cu^+ after excess treatment of H_2Q.   Finally, the obtained H_2Q-HK crystals were dried under vacuum before use.   The entire process was conducted under an inert atmosphere in a moisture-free argon-charged glove box.

Acid or base treatment of H₂Q-treated HKUST-1. To check if the H₂Q-HK crystals shows their structural integrity under acid and base conditions, we immersed the H₂Q-HK crystals into diluted HCl or NH₄OH solution which pH value was adjusted to 3, 5, and 9, respectively. These stability checks were conducted at room temperature.

Sample preparation for the measurements of Raman and UV-vis absorption spectra. Before taking Raman and UV-vis absorption spectra of HKUST-1 samples, we transferred the samples into a moisture-free argon-charged glove box. Then, the samples were contained in disc-shaped quartz cells (Starna, Type 37GS Cylindrical Cells with Quartz to Borofloat graded seal). The quartz cells were also sealed with a glass cork and grease (Apiezon, H high-temperature Vacuum Greases) before the measurements.

Sample preparation for the ¹H-NMR measurements. For the ¹H NMR measurement of HKUST-1 samples, a tiny amount of HKUST-1 sample was dissolved in 1 mL of D_2SO_4. Then, the solution was transferred into an NMR tube. For the ¹H NMR measurement of the supernatant solution after H₂Q treatment (see Figure 3a), a tiny amount of the supernatant solution was diluted in 1 mL of CD_3CN. Then, the solution was transferred into an NMR tube. These processes were also conducted in an argon-charged glove box. Finally, the analyte-containing NMR tubes were sealed with plastic caps and acrylic Parafilm® prior to the measurements.

Instrumentation. DDW was obtained from a water purification system (Merck Millipore, MQ Direct 8). Powder X-ray diffraction (PXRD) patterns were obtained using a PANalytical diffractometer (Empyrean) equipped with a monochromatic nickel-filtered Cu K_α beam. ¹H-NMR spectra were recorded on an AVANCE III HD FT-NMR spectrometer (Bruker, 400 MHz for ¹H). The ¹H chemical shifts were referenced to the residual proton resonance of the solvent. Infrared (IR) absorption spectra were obtained using an FT-IR Microscope (Thermo Scientific, Nicolet Continuum). Scanning electron microscopy (SEM) images were obtained from an FE-SEM (Hitachi S-4800) operated at an acceleration voltage of 3 kV, after samples were coated by Au-Pt alloys with a thickness of approximately 3 nm. Transmission electron microscopy (TEM) images were obtained from a field-emission transmission electron microscope (Hitachi HF-3300) operated at an acceleration voltage of 300 kV. X-ray photoelectron spectroscopy (XPS) analysis was performed using an X-ray photoelectron spectrometer (Thermo Scientific, ESCALAB 250Xi). The single crystal X-ray diffraction (SCXRD) analysis was performed using a diffractometer setup with a Pt-coated Si double-crystal monochromator and an ADSC Q210 CCD detector in the Pohang Accelerator Laboratory (PAL). X-ray absorption near edge structure (XANES) analysis was also performed on the 7D beamline in the Pohang Accelerator Laboratory. The calibration of energies for the samples was carried out by the Cu foil ($E_0 = 8979.0$ eV), and the monochromatic X-ray was obtained by using a Si[111] monochromator. The intensity of the incident (I_0) and transmitted (I_t) X-ray beam in the Cu K-edge was continuously monitored at room temperature, using ionization chambers purged with N_2 including the trace amount of He. The XANES spectra of CuO and Cu_2O were also recorded for the use as references. All recorded spectra were analyzed with the software of IFEFFIT packages (ver. 1.2.11). Diffuse reflectance UV-vis absorption spectra of samples were recorded using an Agilent Cary 5000 UV-VIS-NIR spectrophotometer. By using a BELSORP-max (BEL Japan, Inc.), N_2 and CO adsorption/desorption isotherms of the samples were obtained at 77 K and 273.15 K, respectively. Optical microscope images were taken using an S43T microscope (Bimeince). Raman spectra were recorded using a DXR™2xi Raman Imaging Microscope (Thermo Scientific). Excitation of the samples was performed by focusing a 532-nm-wavelength laser beam. The hydrolytic stability test of the samples was performed by controlling temperature and humidity with a Temperature & Humidity Chamber (Jeio Tech, TH-ME-025).

Section S4. ^{1}H NMR and EPR Spectra of Supernatant Solutions After H$_2$Q-Treatment of HKUST-1

For the H$_2$Q treatment of HKUST-1, we added dehydrated HKUST-1 crystals into H$_2$Q solution, which was prepared by dissolving H$_2$Q in anhydrous acetonitrile (MeCN) with the stoichiometry of 1:2 in the ratio of H$_2$Q:Cu^{2+}, and kept the reaction at 80 °C for 12 h.   Then, we examined ^{1}H NMR measurements with the supernatant solution obtained from H$_2$Q treatment to monitor that H$_2$Q converts to benzoquinone (Q) after donating electrons to Cu^{2+} ions.   The ^{1}H NMR spectra in Figure 3a and Figure S4 show that approximately 15% of H$_2$Q turned to Q after the reaction.   This implies that 30% of Cu^{2+} ions were reduced to Cu$^+$ ions. For the complete conversion of Cu^{2+} ions to Cu$^+$ ions, we repeated the above process 5 times.   Interestingly, however, the reaction did not further proceed (see Figure S4 below).

Meanwhile, a reviewer asked us to prove the generation of quinhydrone radical (HQ$^\bullet$).   We estimated that the HQ$^\bullet$ radical can be formed after H$_2$Q donates an electron to Cu^{2+} ion.   However, we also estimated that the complexed HQ$^\bullet$ radical pairs (quinhydrone pairs) seem to be in an equilibrium state with a mixture of hydroquinone and benzoquinone through the disproportionation reaction of the radical pairs because such chemical substances are dissolved in a polar solvent, MeCN (see Figure S5 below).   To address the above question, we examined the electron paramagnetic resonance (EPR) with a supernatant solution obtained after H$_2$Q treatment.   For comparison, we also examined a commercial quinhydrone after dissolving it in MeCN. However, we could observe no peak in the EPR spectra (see Figure S6 below).   From this observation, we tentatively concluded that the formed HQ$^\bullet$ radicals are converted to hydroquinone and benzoquinone via the disproportionation reaction.
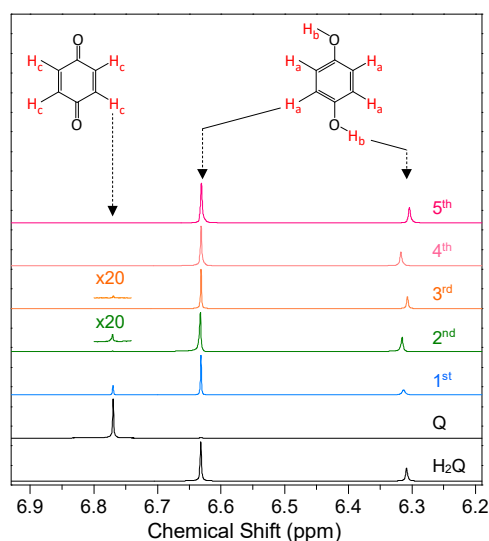
Figure S4. ^{1}H NMR Spectra of a commercial H$_2$Q (blue) and Q (green) dissolved in MeCN and supernatant solutions obtained after H$_2$Q treatment of HKUST-1.   All ^{1}H NMR spectra were obtained after the samples were diluted in deuterated acetonitrile, CD$_3$CN.
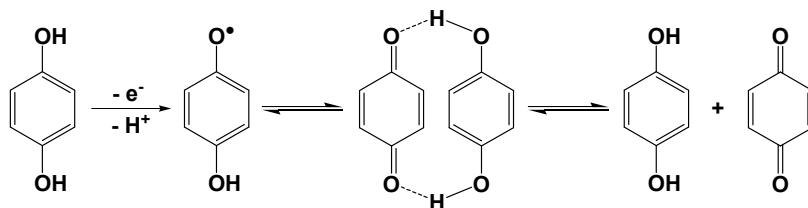

Figure S5. Schematic representation for the disproportionation reaction of HQ$^\bullet$ radical pair into H$_2$Q and Q.
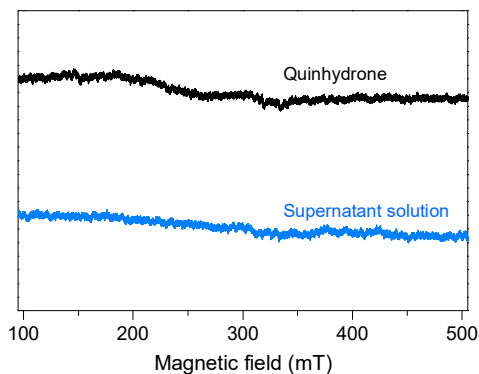
Figure S6. EPR Spectra of a commercial quinhydrone (HQ) and a supernatant solution obtained after H₂Q treatment of HKUST-1. All EPR spectra were obtained after the samples were diluted in acetonitrile.

Section S5. XPS and XANES Analysis of Commercial CuO and Cu₂O

To corroborate the chemical shifts of Cu^{2+} and Cu^{+} ions in the XPS and XANES spectra of HKUST-1 and H₂Q-treated HKUST-1, we also examined the commercial CuO and Cu₂O samples. As results, the chemical shifts of HKUST-1 and H₂Q-treated HKUST-1 agree well with those of CuO and Cu₂O (see Figure S7 below)
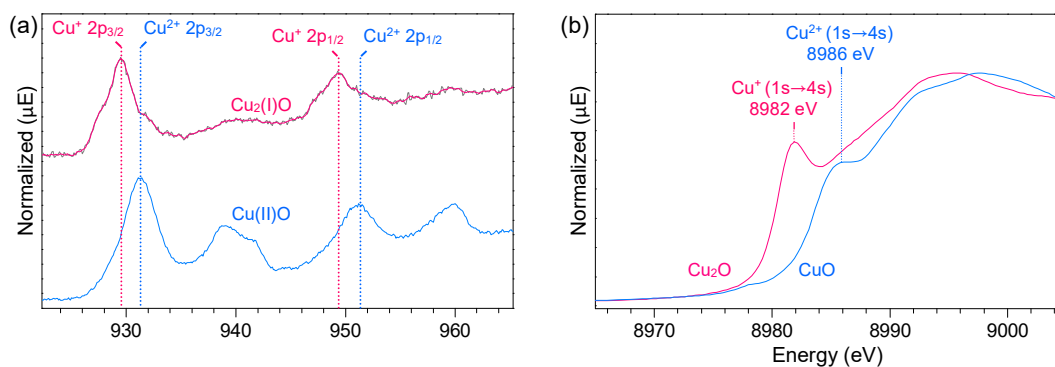
Figure S7. (a) XPS and (b) XANES spectra of commercial Cu₂O and CuO crystals.

Section S6. SEM Analysis of HKUST-1 Samples Before and After H₂Q Treatment
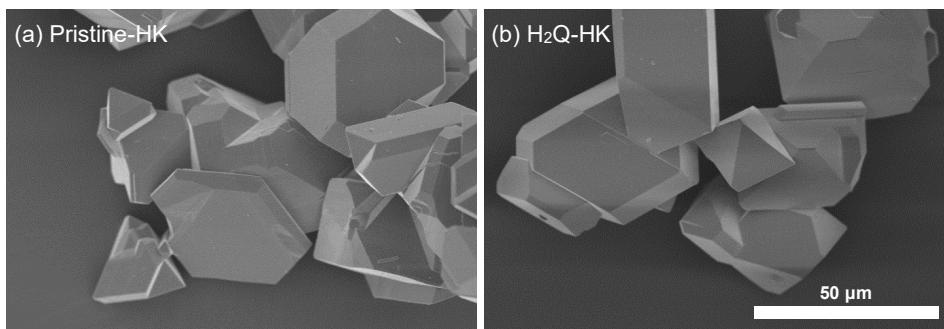
Figure S8. SEM images of (a) pristine HKUST-1 and (b) H₂Q-treated HKUST-1 samples.

Section S7. Single Crystal Structure of H₂Q-Treated HKUST-1

To obtain the crystal structures of pristine HKUST-1 and H₂Q-treated HKUST-1, first, we coated the single crystals with paratone-*N* oil. The X-ray diffractions were obtained at 100 K by using silicon (111) double crystal monochromator (DCM), synchrotron radiation with the wavelength (λ) of 0.61000 Å, and ADSC Q210 CCD and Rayonix MX225HS detectors for pristine-HK and H₂Q-HK, respectively, which are installed at BL2D-SMC beamline in the PAL. Using PAL BL2D-SMDC software,[S2] the diffraction data were collected in every one second for a frame at the detector distance of 63 mm (for pristine-HK) and 66 mm (for H₂Q-HK) with the omega scan ($\Delta\omega$) of 2°. Also, a software of HKL3000sm (Ver. 716.7)[S3] was used for the cell refinement, reduction, and absorption correction. Then, the crystal structures of pristine-HK and H₂Q-HK were solved by the intrinsic phasing method with software of the SHELXT-2018[S4] and subsequently, refined by full-matrix least-squares calculations with software of the SHELXL-2018.[S5] All atoms except hydrogen were refined, considering the atomic anisotropy. Hydrogen atoms bound to carbon atoms in the benzene moieties were considered to place at geometrically ideal positions and constrained to ride on their parent atoms with the C−H bond length of 0.95 Å and the $U_{iso}(H)$ value of 1.2 U_{eq} for the parent atoms. As for pristine-HK, the hydrogen atoms in the coordinated water molecule were considered to locate in difference maps and restrained with the O−H bond length of 0.90 – 1.008 Å by using DFIX and DANG commands. As for H₂Q-HK, the MeCN molecule coordinated at Cu²⁺ was identified, using subsequent Fourier synthesis. The occupancy of atoms in the Cu²⁺−coordinated MeCN was constrained with the value of approximately 70%, based on the results obtained from CO adsorption and ¹H NMR (see the main text). Also, the geometry of the MeCN was restrained by using the functions of DFIX, DANG, ISOR, SIMU and DELU in SHELXL commands. Although pore-filling solvents were observed in the X-ray diffraction, the exact position of the solvent molecules could not be defined due to the disorder of their electron densities. Using the SQUEEZE program installed in the software of PLATON,[S6] we performed the final structural refinements. The refinements were also performed on the basis of the structure factors and the contribution of disordered solvent molecules. The finally converged *R*-factors for the structure of pristine-HK were R1 = 0.0342 and wR2 = 0.0977 for 1142 reflections with I > 2σ(I) and R1 = 0.0399 and wR2 = 0.100 for all reflections, respectively. In the case of pristine-HK, the largest differences in peak and hole were 0.813 and −0.439 e·Å⁻³, respectively. The finally

converged *R*-factors for the structure of H$_2$Q-HK were R1 = 0.0696 and wR2 = 0.2386 for 1302 reflections with I > 2σ(I) and R1 = 0.0721 and wR2 = 0.2407 for all reflections, respectively.　In this case, the largest difference in peak and hole were 1.775 and −1.342 e·Å^{-3}, respectively.

Table S1. Crystal data and structure refinement for pristine-HK and H$_2$Q-HK.

Identification code	Pristine-HK		H$_2$Q-HK	
Empirical formula	C$_{144}$H$_{96}$Cu$_{24}$O$_{120}$		C$_{209.60}$H$_{146.40}$Cu$_{28}$N$_{32.80}$O$_{96}$	
Formula weight	5271.16		6439.54	
Temperature	100(2) K		100(2) K	
Wavelength	0.610 Å		0.610 Å	
Crystal system	Cubic		Cubic	
Space group	*Fm-3m*		*Fm3m*	
Unit cell dimensions	a = 26.274(3) Å	α= 90°.	a = 26.303(3) Å	α= 90°.
	b = 26.274(3) Å	β= 90°.	b = 26.303(3) Å	β= 90°.
	c = 26.274(3) Å	γ= 90°.	c = 26.303(3) Å	γ= 90°.
Volume	18137(6) Å^3		18197(6) Å^3	
Cu−O$_{BTC}$ distance	1.950 Å		1.955 Å	
Z	2		2	
Density (calculated)	0.965 Mg/m^3		1.175 Mg/m^3	
Absorption coefficient	0.944 mm^{-1}		1.096 mm^{-1}	
F(000)	5232		6427	
Crystal size	0.315 x 0.305 x 0.298 mm^3		0.135 x 0.125 x 0.118 mm^3	
Theta range for data collection	1.152 to 24.986°.		1.329 to 24.997°.	
Index ranges	-36<=h<=36, -36<=k<=36, -36<=l<=36		-36<=h<=36, -36<=k<=36, -36<=l<=36	
Reflections collected	40493		39965	
Independent reflections	1315 [R(int) = 0.0765]		1302 [R(int) = 0.0969]	
Completeness to theta = 21.469°	99.3 %		97.6 %	
Absorption correction	Empirical		Empirical	
Max. and min. transmission	1.000 and 0.946		1.000 and 0.883	
Refinement method	Full-matrix least-squares on F^2		Full-matrix least-squares on F^2	
Data / restraints / parameters	1315 / 2 / 39		1302 / 36 / 58	
Goodness-of-fit on F2	1.111		1.181	
Final R indices [I>2sigma(I)]	R1 = 0.0342, wR2 = 0.0977		R1 = 0.0696, wR2 = 0.2386	
R indices (all data)	R1 = 0.0399, wR2 = 0.1000		R1 = 0.0721, wR2 = 0.2407	
Extinction coefficient	0.00042(6)		n/a	
Largest diff. peak and hole	0.813 and -0.439 e.Å^{-3}		1.775 and -1.342 e.Å^{-3}	

Section S8. IR Spectra of Commercial $[Cu(MeCN)_4]BF_4$ Complex Before and After Hydration
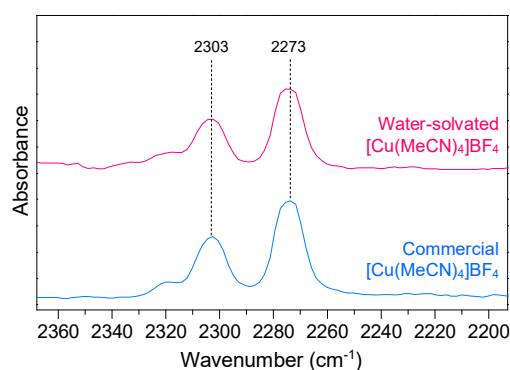
Figure S9. IR spectra of a commercial $[Cu(MeCN)_4]BF_4$ sample before (blue) and after (pink) hydration. The spectra show that the ionic $[Cu(MeCN)_4]^+$ complex is inert although the complex is hydrated with H_2O.

Section S9. Calculations of Theoretical and Experimental Values Regarding Cu^{2+} Reduction

Table S2. Theoretical ratio of small cages to Cu^{2+} ions and the theoretical maximum amount of Cu^{2+} reduction

Term	Value
Theoretical number of small cages in a unit cell of pristine HKUST-1[a]	8
Theoretical number of Cu^{2+} ions in a unit cell of pristine HKUST-1[a]	48
Theoretical number ratio of small cages to Cu^{2+} ions in HKUST-1[a]	$0.166_7 \, (= 8/48)$
Theoretical percent value for the formation of $[Cu^I(MeCN)_4]$ complex (mol%)[b]	16.6_7
Theoretical percent value for total Cu^{2+} reduction (mol%)[b]	**33.3**

[a]See Figure 1 and Figure 4b
[b]Considering that the reduction process should be thermodynamically stable

Table S3. Calculation for the mole percent of framework Cu^+ ions based on CO adsorption experiment

Term	Calculation	Calculation result
Amount of adsorbed CO (CO mmol/HK g)		0.730
Mw of Cu_3BTC_2 unit (g/mol)		604.9
Mole of Cu_3BTC_2 unit per 1 g of HK (HK mmol/HK g)	$(1 \text{ g}/604 \text{ g mol}^{-1}) \times 10^3$	1.656
Mole of CO per mole of Cu_3BTC_2 unit (CO mmol/ HK mmol)	0.730 mmol/1.656 mmol	0.441
Number of Cu^{2+} in a Cu_3BTC_2 unit		3
Mole fraction of CO per total Cu sites (CO mol/ Cu sites mol)	0.441/3	0.147
Mole percent of the formed framework Cu^+ in HK (mol%)		**14.7 mol%**

Table S4. Theoretical ratio of protons in BTC ligand to protons in MeCN coordinated at Cu^{2+} in H_2Q-HK

Term	Value
Mole ratio of BTC to Cu in a Cu_3BTC_2 unit of pristine HK	2:3
Mole ratio of BTC to Cu in a Cu_3BTC_2 unit of H_2Q-HK[a]	2:2
Number of ^1H in BTC	3
Number of ^1H in MeCN	3
Number of ^1H of BTC in a Cu_3BTC_2 unit of H_2Q-HK	6
Number of ^1H of MeCN in a Cu_3BTC_2 unit of H_2Q-HK	6
Number ratio of ^1H in BTC to MeCN in a Cu_3BTC_2 unit of H_2Q-HK[a]	**6:6 (= 1:1)**

[a]33.3 mol% Cu^{2+} ions are reduced to Cu^+ ion, and thereby 66.7 mol% Cu^{2+} ions remain in H_2Q-HK.   So, 3 (for Cu) × 0.667 = 2

Table S5. Calculation for the mole percent of $[Cu(MeCN)_4]^+$ complex in H_2Q-HK based on ^1H NMR

| Term	Value
Mole ratio of BTC to Cu in Cu_3BTC_2 unit (BTC:Cu)	2:3
Number of ^1H in BTC	3
Number of ^1H in $[Cu^I(MeCN)_4]$ complex	12
[a]Mole ratio of ^1H in $[Cu^I(MeCN)_4]$ to ^1H in BTC (^1H in $[Cu^I(MeCN)_4]$ / ^1H in BTC)	6 (= 36/6)
[b]Obtained mole ratio of ^1H in $[Cu^I(MeCN)_4]$ complex to ^1H in BTC^{3-}	0.94
Mole fraction of $[Cu^I(MeCN)_4]$ complex to the total number of Cu	0.157 (= 0.94/6.0)
Mole percent of $[Cu^I(MeCN)_4]$ complex to the total number of Cu (mol%)	**15.7**

[a]Calculated ideal value for the mole ratio of protons in $[Cu^I(MeCN)_4]$ to in BTC, by an assumption, if all Cu^{2+} is converted to $[Cu^I(MeCN)_4]$ complex.
[b]Real value obtained from a ^1H NMR result shown in Figure 5d.

## Section S10. Stability Check for HKUST-1 After CO Adsorption
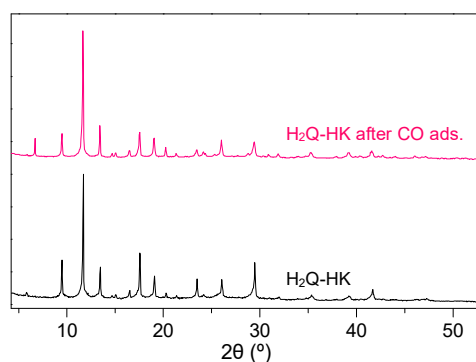
Figure S10. PXRD patterns of H_2Q-HK before (black) and after (pink) the measurement of CO adsorption isotherms.

## Section S11. Raman Study with pristine-HK and H₂Q-HK Samples
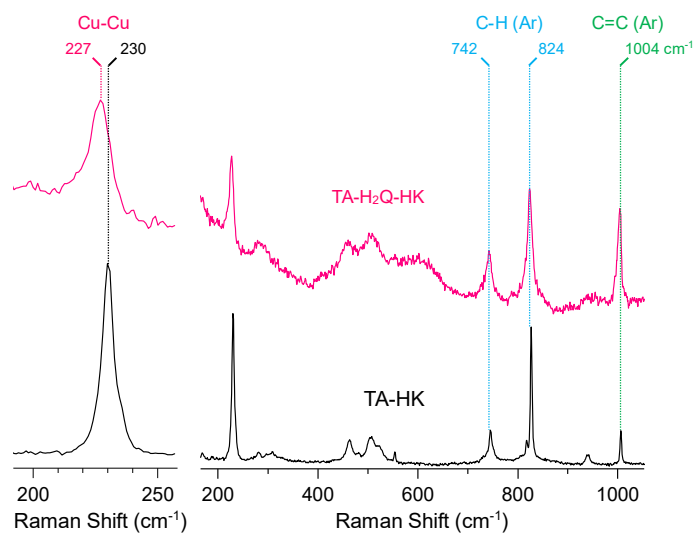
Figure S11. Raman spectra of thermally activated pristine-HK (black curve) and H₂Q-HK (pink curve). The intensity ratio of Raman peak at 230 cm^{-1} for Cu^{2+}–Cu^{2+} stretching vibration of pristine-HK and H₂Q-HK is approximately 0.5.

Section S12. SEM Observation of Pristine and H₂Q-Treated HKUST-1 Samples Before and After Exposure to Water
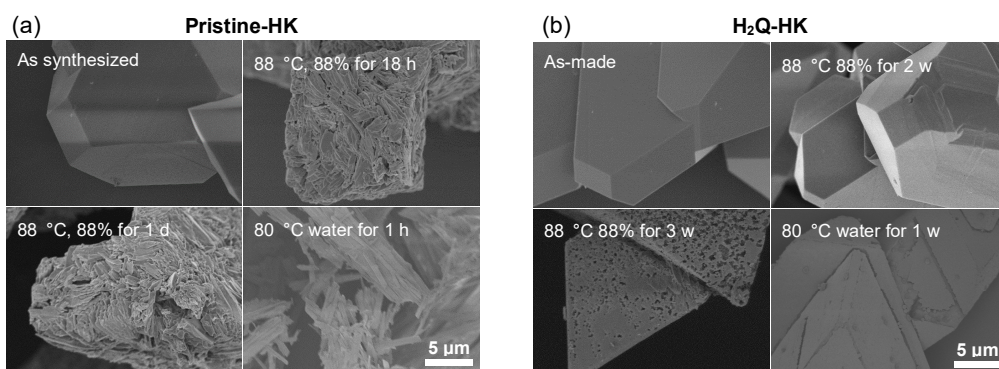
Figure S12. SEM images of (a) pristine-HK and (b) H₂Q-HK samples before and after exposure to humid air or water.

Section S13. PXRD Patterns of H₂Q-HK Samples After Acid or Base Treatments
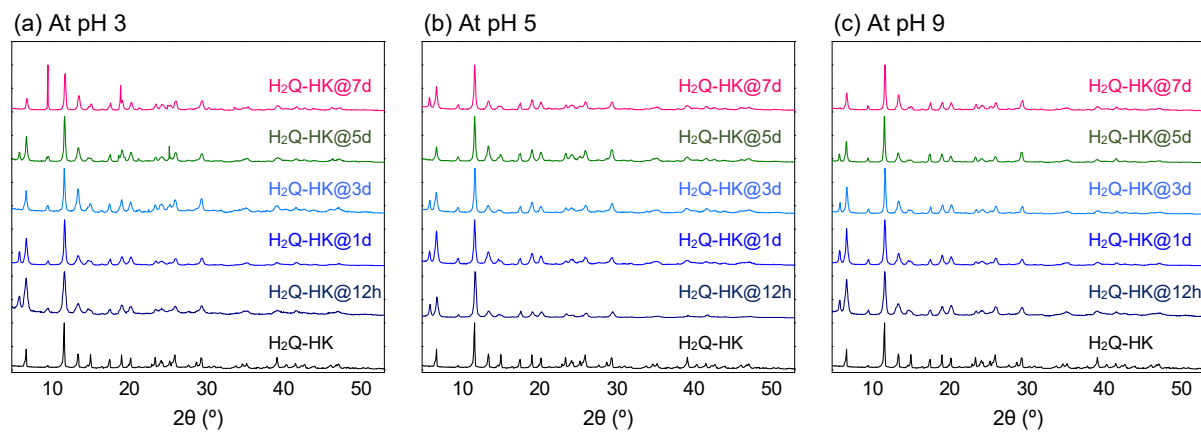
Figure S13. PXRD patterns of H₂Q-treated HKUST-1 powder samples after acid or base treatments at pH (a) 3, (b) 5, and (c) 9.

References

S1. Bae, J.; Choi, J. S.; Hwang, S.; Yun, W. S.; Song, D.; Lee, J. D.; Jeong, N. C. Multiple Coordination Exchanges for Room-Temperature Activation of Open-Metal Sites in Metal-Organic Frameworks. *ACS Appl. Mater. Interfaces* **2017**, *9,* 24743-24752.

S2. Shin, J. W.; Eom, K.; Moon, D. BL2D-SMC, the supramolecular crystallography beamline at the Pohang Light Source II, Korea. *J. Synchrotron Rad.* **2016**, *23,* 369-373.

S3. Otwinowski, Z.; Minor, W.; *In Methods in Enzymology*, ed. Carter, Jr., C. W.; Sweet, R. M. Academic Press, New York, 1997, vol. 276, part A, pp. 307.

S4. Sheldrick, G. M. SHELXT - Integrated space-group and crystal-structure determination. *Acta Cryst.* **2015**, *A71,* 3–8.

S5. Sheldrick, G. M. Crystal structure refinement with SHELXL. *Acta Cryst.* **2015**, *C71,* 3–8.

S6. Spek, A. L. Structure validation in chemical crystallography. *Acta Cryst.* **2009**, *D65,* 148-155. (for Platon program)